Author/s:
Li, J;Dyer, A;Smith, D;Mulvaney, P

Title:
Gold Nanodrum Resonators

Date:
2023-10-24

Citation:
Li, J., Dyer, A., Smith, D. & Mulvaney, P. (2023). Gold Nanodrum Resonators. ACS Nano, 17 (20), pp.20551-20559. https://doi.org/10.1021/acsnano.3c07334.

Persistent Link:
https://hdl.handle.net/11343/338755

Gold Nanodrum Resonators

Jialu Li,[†] Ash Dyer,[‡] Dan Smith,[‡] and Paul Mulvaney[*,†]

†*ARC Centre of Excellence in Exciton Science, School of Chemistry, the University of Melbourne, Parkville, VIC., 3010, Australia.*

‡*Melbourne Centre for Nanofabrication, 151 Wellington Road, Clayton, VIC., 3168, Australia*

E-mail: mulvaney@unimelb.edu.au

Phone: +61 (0)3 8344 2429. Fax: +61 (0)3 9348 1595

Abstract

Nanodrum resonators have been fabricated using nanometre thick gold films as the drumheads. The fabrication method is favourable for large-area array manufacture of arbitrary shapes. The drum resonators exhibit fundamental mode vibration frequencies in the MHz regime. We use the stretched-plate model to describe the natural vibrations of the drum. The Q factor of the fundamental mode increases as the thickness of the drum increases and decreases as the drum diameter goes up. The highest Q factor of the fundamental mode reaches 290 at room temperature and atmospheric pressure. Based on the deduced material properties we estimate that the resonator has a mass sensitivity of 1.11×10^{-22} g/Hz.

Keywords: Gold, thin film, drum resonator, NEMS, mass sensing

Introduction

Nanoelectromechanical resonators have applications as ultrasensitive mass sensors,[1,2] accelerometers,[3] electromechanical signal processors[4–6] and even as gravimeters.[7] A variety of

such devices have been reported based on beam geometries and using materials such as carbon nanotubes ,[8,9] metal nanowires ,[10] or silicon nanowires [11,12] as the resonating materials. An alternative to beams is to use 2-dimensional materials which can readily form nanodrum resonators with monolayer graphene being of particular interest .[13–15] A key feature of these drumheads is that the transferred films usually bind very strongly via van der Waals forces such that the suspended film can be viewed as "clamped at the edge" .[16] The adhesion creates a completely sealed chamber .[17] Devices based on graphene, monolayer transition metal dichalcogenides [18,19] and their heterostructures[20] have also been investigated. Such drum-like resonators display relatively high resonance frequencies compared with beams of similar scales and can perform as pressure sensors or gas filters .[21,22] Although these electromechanical prototypes show high resonance frequencies and good Q factors, the fragility of 2-dimensional materials and the difficulty in transferring and manipulating them has thus far limited their practical application. In view of this, we propose using evaporated metal films as drumheads. The thickness and composition of such films is highly reproducible and tunable.

Here we present a nanoelectromechanical resonator using only nanometre-thick gold films as the drumhead. Suspended pure gold thin films of various shapes and sizes are achieved by a semi-dry transfer method, which also facilitates systematic study of the dimension dependence of the mechanical response of the drum resonator. The sizes of the drums range from 1 to 10 microns (diameter for circular ones and side lengths for square ones). We show that the gold films exhibit only nanometre scale "droop" despite aspect ratios, AR (= length/thickness) of nearly 1,000 and typically these films evince a fundamental mechanical mode in the MHz regime. The quality of the films can be easily evaluated by optical microscope. The fabrication method introduced here is potentially scaleable and the composition of the drumhead can be readily tuned to optimise the optical, mechanical and electrical response.

Results and discussion

Figure 1 **a** depicts the design of the gold nanodrums and the resonance behaviour characterisation. The substrates are fabricated by photolithography followed by reactive ion etching, and the gold films are first deposited on a Si/SiO_2 chip and then transferred onto the patterned substrates by a semi-dry transfer method. See Methods and **Supporting Information** (Figure **S1**) for details. The underlying substrate is n-doped silicon with a DC electronic resistivity of 1-10 Ω-cm; this layer can act as a back electrode. The top gold film is highly conductive, which allows electric signals to be applied. Except for the natural vibration induced by the intrinsic properties of the films, i.e., tension and flexural rigidity, the response of the gold film to arbitrary electric signals can be studied as well. The resonance frequencies are measured using laser Doppler vibrometry. Two vibrometers were used in these experiments, namely the Polytec MSA-400 (range 0-25 MHz) and Polyetc UHF-120 (range 25-100 MHz) depending on the target frequency range. All the spatial scans of the drumheads were performed with the Polytec MSA-400. The fabrication method employed here is favourable for fabricating large arrays of nanodrums of various sizes and shapes. Figure 1 **b** presents microscope images of circular gold drums of different sizes (diameter from 1 µm to 10 µm). We can see that the surface is uniform and undamaged. The drum area is distinctly different in colour from the surrounding substrate. Figure **S2** shows a microscope image of an empty well patterned on the Si/SiO_2 substrate before gold film transfer for comparison. The corresponding SEM images in Figure 1 **c** show that the film is suspended over the well. Figure 1 **d** shows the topography of a drum determined by tapping mode AFM and Figure 1 **e** presents the corresponding section profile taken along the white dashed line in **d, i** and **ii**, which is an empty well of the same dimensions. It can be seen that the well is 298 nm deep and the gold film droops by about 26 nm. Figure **S3** shows images of a random drum of each diameter from 2 µm to 9 µm and we plot the droop at the centres vs the diameter in Figure **S4**. It shows that the droop is similar in magnitude, irrespective of the size of the drum. Figure **S5** shows microscope images of gold nanodrums of various

shapes. The damaged drums are circled out, and these display distinctly different colours to the working drums. Therefore, we can identify whether a drum is damaged simply by using optical microscopy, rather than using more sophisticated techniques, such as TEM or AFM, which are usually more damaging and time-consuming.

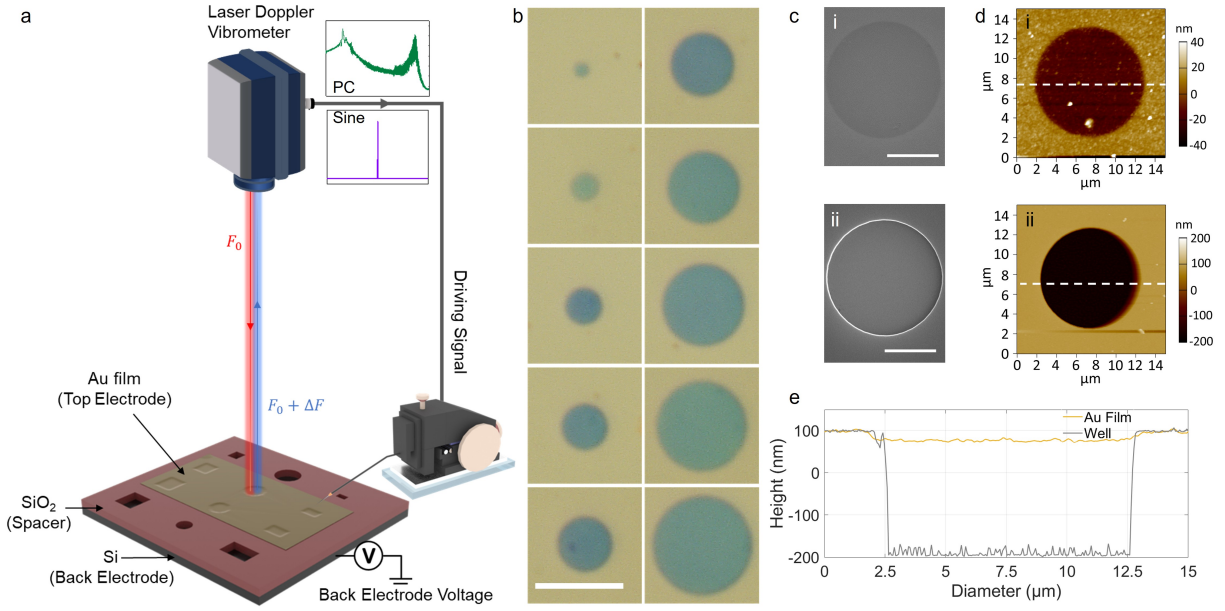

Figure 1: The gold nanodrum resonator and the morphology characterisation. (a) Schematic of the gold nanodrum resonators and the resonance characterisation method. The frequency is detected by the Doppler shift of the incident laser induced by the vibration of the drumheads. Two types of electronic signals are employed in this work. Periodic chirp (PC) signals are used for highlighting the natural resonance frequencies of the drums whereas sinewaves are used for investigating the ability of a drum to output arbitrary electronic signals. (b) Microscope images of gold nanodrums of different diameters. Scalebar: 10 µm (c) SEM images of (top) a gold nanodrum and (bottom) an empty well on the Si/SiO_2 substrate. (For microscope images of the empty well see Figure S2). Scalebar: 5 µm. (d) AFM topography images of (top) a gold nanodrum and (bottom) an empty well. (e) cross sections of the drums at the points corresponding to the white dashed lines in Figure d. The thickness of the gold film in of all the drums presented in this figure is 28 nm.

Figure 2 (a) shows vibration spectra collected along the diameter of a 10-micron drum with a 28 nm-thick gold film. The white dashed lines denote the edges of the drum and the yellow dashed line denotes the centre of the drum. The vibration was excited electrostatically by a periodic chirp signal with a peak amplitude of 5 V and offset of 5 V, as shown in Figure **S6**. The spectra were collected with the Polytec MSA-400 vibrometer and the contour image

is constructed from 29 sets of spectra. It can be seen that different spots on the drum surface exhibit different vibrational modes. The very centre of the drum participates in the most numbers of modes. We take the individual spectrum of the orange dashed line, i.e., the centre of the drum and plot it in (b). In the range of 0-25 MHz, 3 resonance peaks are most notable. We use (m,n) to denote the resonance modes, where m refers to the number of nodal lines in the radial direction and n to the number in the azimuthal direction. The two indices also correspond to the n-th root of the m-order Bessel function, which is discussed in more detail in **Section 2** of the **Supporting Information**. The insets show the vibration shapes of the membrane at different peak frequencies taken from scans with the Polytec MSA-400; these shapes correspond to the (0,1) mode, (0,2) mode and (0,3) mode. To ensure that the periodic chirp signal has no influence on the values of the eigenfrequencies, we collected spectra at the same position on the drum using 7 different periodic chirp signals and the frequencies of the three modes are plotted in Figure **S7**. One can see that the 3 modes only deviate in frequency by at most 11 % and no clear trend can be detected. Likewise when the back voltage was altered within the range of 0-10 V, there were no significant shifts in the resonance frequencies.

Regardless of the amplitude or shape of the chirp signal, not all of the expected modes of the drumheads could be observed. In principle, at the position of $a/2$ or $3a/2$ (where a denotes the radius), we should be able to detect (1,1), (1,2) or (2,1) modes .[23,24] These modes are displayed in Figure **S8**. However, the only detectable modes experimentally are those with 0 nodal lines. That may be due to the fact that to excite an azimuthally asymmetrical ($m \neq 0$) mode requires countermotions of the two halves (or four quarters) of the membrane in opposite directions. However, this would require that the different regions of the drumhead are at different electric potentials, which is difficult to achieve with electrostatic excitation.

For a thin circular film with clamped edges, the mechanical properties depend upon the flexural rigidity of the material and the inbuilt tension. If the rigidity dominates, then plate theory may be applied, whereas if the inbuilt tension dominates, the mechanics obey those

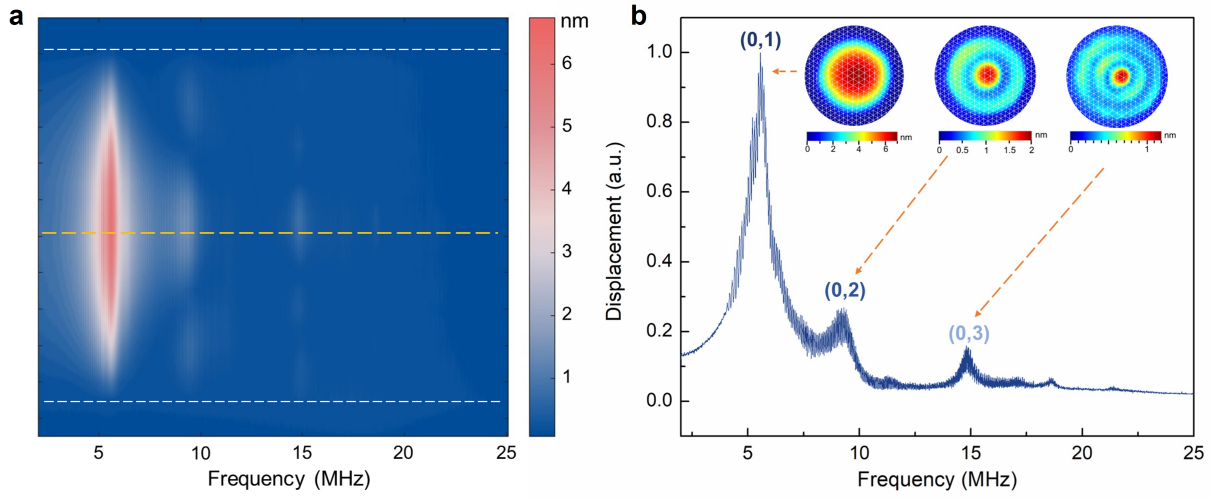

Figure 2: Natural vibration spectra and modes of an individual drum. (a) Resonance spectra at different points along the diameter of a drum with a diameter of 10 µm. The thickness of the gold film is 28 nm. The contour image is constructed from 29 sets of data using Matlab. The white dashed lines denote the drum area and the yellow dashed line shows the centre of the drum. (b) Resonance spectrum at the yellow dashed line in (a). The insets show different mode shapes at different resonance frequencies. The electrical signal applied to the gold film is a periodic chirp signal with an amplitude of 5 V and offset of 5 V. Back voltage is 0 V.

of a membrane.

To describe both regimes with one equation, we use the stretched-plate model.[25] By defining $\mathcal{A} = Td^2/4\mathcal{D}$, we can write the predicted vibration frequency as

$$f_{mn} = \frac{2k_{mn}}{\pi d^2}\sqrt{\frac{\mathcal{D}}{\rho}(k_{mn} + \mathcal{A})}, \tag{1}$$

where d is the diameter, ρ is the surface mass density, and $\mathcal{D} = Eh^3/[12(1-\nu^2)]$ is the flexural rigidity. Here h is the thickness of the gold film, E is the Young's Modulus, and ν is the Poisson ratio. k_{mn} are eigenvalues of the differential equation describing the vibration for any given $\mathcal{A}$. It can be seen that when $\mathcal{A} \to \infty$, the equation simplifies to that of an ideal membrane, i.e.,

$$f_{mn} = \frac{k_{mn}^{\mathrm{M}}}{\pi d}\sqrt{\frac{T}{\rho}}, \tag{2}$$

where k_{mn}^{M} are the eigenvalues for the membrane case. Notably, the frequency varies as $1/d$ and is independent of the drum head thickness. A difficulty with nanoscale drums is determining the inbuilt tension.

Conversely, when $\mathcal{A} \to 0$, the equation approaches the ideal plate regime,

$$f_{mn} = \frac{2(k_{mn}^{\mathrm{P}})^2}{\pi d^2}\sqrt{\frac{\mathcal{D}}{\rho}}, \tag{3}$$

where k_{mn}^{P} is the eigenvalue for the plate model. In this regime, the vibration is dominated by the rigidity and the frequency is strongly dependent on the thickness of the film. It also now depends on $1/d^2$.

For more details of the differential equations describing the vibration of a drumhead and the determination of k_{mn}, see **Section 2.1** of the **Supporting Information**.

Since all of the drums exhibit a fairly uniform degree of droop (Δ), considering the stress dependence of the sizes of the drums, the tension can be written as a function of the diameter in the form of

$$T(d) = \frac{(d^2 + \Delta^2)}{(d_0^2 + \Delta^2)}T_0 \approx \frac{d^2}{d_0^2}T_0, \tag{4}$$

where d_0 is the largest diameter, in our case 10 µm, T_0 is the tension of the largest drumhead (**Section 2.2, Supporting Information**).

To investigate the vibrational response of the drums, we measured the eigenfrequencies of samples of different diameters and thicknesses, as defined in Figure 3 (a). Figure 3 (b) presents spectra taken at the centres of drums with diameters ranging from 2 µm to 10 µm. The signals from 1 µm diameter drums could not be detected due the large laser spot size. The colour is proportional to the intensity of the signal. It is evident that the intensity of the modes decreases drastically as the order of the modes goes up. The frequencies of all of the modes shift to higher frequencies as the diameter decreases. Within the frequency range below 25 MHz, only for drums bigger than 5 µm, can the (0,3) modes be detected

with the vibrometer. Figure 3 (c) and (d) display these graphical data as plots of frequency vs diameter for the first three modes. Drums ranging from 2 µm to 10 µm in diameter with thicknesses of either 28 nm or 110 nm were used, to ensure a sufficient range of aspect ratios and $\mathcal{A}$ values were sampled. It can be seen that for both thicknesses, the frequencies scale inversely with the diameter and increase with the thickness. As the diameter of the drums increases, the value of $\mathcal{A}$ also increases and the influence of the thickness on the vibration frequencies fades away and the vibration behaviour becomes more membrane-like. Conversely, as the size of the drums shrinks, the frequencies become more strongly dependent on the thickness, making it more plate-like. We extracted the tension as 2.71 N/m for a 10 µm drum with a 28 nm thick gold film, which is the most membrane-like sample. The stretched-plate model provides a good fit, albeit with an effective Young's modulus of around 22 GPa, which is much lower than that of bulk gold. However, it has been reported that the Young's modulus of thin gold films is lower than the bulk value, and that it is also dependent on the crystallinity and facets present.[26,27] The Young's modulus of films deduced from vibration frequencies are often much lower than those determined by other techniques such as nanoindentation.[28–31] Table **S1** provides a comparison of values of the Young's modulus for different film materials determined by various methods. The relatively low Young's modulus may suggest that the boundary conditions of the drumheads is more complicated than the clamped case. Assuming that the Young's modulus varies little with thickness in the nanometre range, we find that the 110 nm thick gold drums with a diameter of 10 µm are subjected to a tension of 5 N/m. We used the same Young's modulus and tension for the (0,2) modes of both thicknesses and (0,3) mode of the 28 nm samples and they all fit very well with experimental data as shown in Figure 3 (d), validating the robustness of the theoretical model. These data imply that the Young's modulus is fairly constant while the inbuilt tension does change with drum diameter according to equation 4. We plot the frequencies of the resonators vs the drum diameters for both thicknesses of the gold films and also the fits derived from the membrane model and the plate model in

Figure **S9**. It is seen that neither mode fits the experimental results well across all sizes. For the 28 nm gold film samples, the membrane model gives a good fit for the drums of 9 µm and 10 µm diameter while the plate model fits the 2 µm and 3 µm ones reasonably. For the 4 µm to 7 µm samples, both regimes fail to describe the trend. Conversely, for the110 nm samples, the plate model gives relatively good fits for most of the diameters, especially at the small end. The membrane model, however, fails to fit any size. The stretched-plate model, which incorporates features from both regime fits the experiments well across the full range of sizes. We have presented all the results from the three models together with the experimental results in Table **S3** and Table **S4**.

This regime-transition is further verified by looking into the effect of thickness. Figure 3(e) shows the spectra taken in the centres of the 3-micron and 5-micron drums of the thicknesses of 20 nm, 30 nm and 110 nm. Though the frequencies of the first modes increases as the thickness goes up for both sizes, the frequency shift for the 3 µm drums (14.05 MHz) is twice as large as that observed for the 5 µm drums (5.96 MHz). We plot the peak frequencies vs thickness in Figure 3(f). (Where the same symbols are used, this denotes that the data were acquired from the same batch of samples, indicating the same T_0.)

We can see that as the thickness changes from 20 nm to 110 nm, the ratio between the fundamental modes of the two diameters ($\mathcal{R} = f_{01}^{3\mu\mathrm{m}}/f_{01}^{5\mu\mathrm{m}}$) does not stay unchanged. (The dashed lines in the figure are just to show that the ratio is not constant. They do not stand for proportional relationships.) At 20 nm, $\mathcal{R} = 1.66$, which is very close to the value in the membrane regime, i.e., $5/3 = 1.67$. Conversely, $\mathcal{R} = 3.29$ when the thickness is 110 nm, which is closer to the value in the plate regime, i.e., $5^2/3^2 = 2.78$.

The ratio of the frequencies for the (0,2) and (0,1) modes provides a further indication of the vibration regime. We plot this ratio as a function of d^4/h^3 as suggested by the stretched-plate model and the tension expressed in Equation **S9**, as shown in Figure **S10**. The orange dashed line indicates the ratio expected according to the pure membrane model while the green dashed line indicates the ratio for the pure plate model. One can see that for most of

the values of $d^4/h^3 (< 30)$, the ratios fall in between the values of these two models, indicating the drums cannot be accurately described by either model. As the value of d^4/h^3 approaches 0, the ratio between the two modes approaches the value of the plate model, indicating that for a small, thick gold film, the actuation force is due to bending rigidity. When the d^4/h^3 is larger than 30, the ratio between the two modes decreases, asymptoting to a value closer to that predicted by the membrane model.

Due to the flexibility of our fabrication approach, the shapes of the drumheads are merely determined by the shapes of the wells on the substrates. Figure 4 shows the vibration behaviours of square drums. The resonance spectra collected in the middle of a square drum with side lengths of 7 µm (Figure 5 (a)) are shown in Figure 4 (b). Three modes can be detected, namely the [1,1], [1,3] (or [3,1]) and [3,5] (or [5,3]) modes, where the numbers correspond to the nodal lines along the two perpendicular edges. The insets display the actual shapes of the modes.

We then investigated the dependence of the eigenfrequencies on the drum thickness and diameter in a similar way to the circular drums. Figure 4 (c) and (d) show the [1,1] and [1,3] (or [3,1]) modes of square drums of different thicknesses and side lengths. One can see that the same trends apply as in the case of circular drums. As the drum becomes larger, the vibration behaviour becomes more membrane-like. As the drum size shrinks down, it becomes more plate-like. Higher-order modes are more plate-like as well. Assuming the 28 nm drum with an edge length of 10 µm to be a perfect membrane, we can calculate that the tension is about 3.11 N/m, which is in line with the value acquired from the circular drum. The membrane and plate frequencies of a square drum are shown in Figure **S11 Section 3** and Table S5 and S6 of the **Supporting Information**.

The resonance spectrum of the fundamental mode taken at room temperature and standard atmospheric pressure from a 110 nm-thick circular drum of the diameter of 2 µm is displayed in Figure 5 (a). The peak is well fit by a Lorentzian function. The centre frequency is located at 42.063 MHz, with a full width at half maximum of 0.18 MHz, corresponding

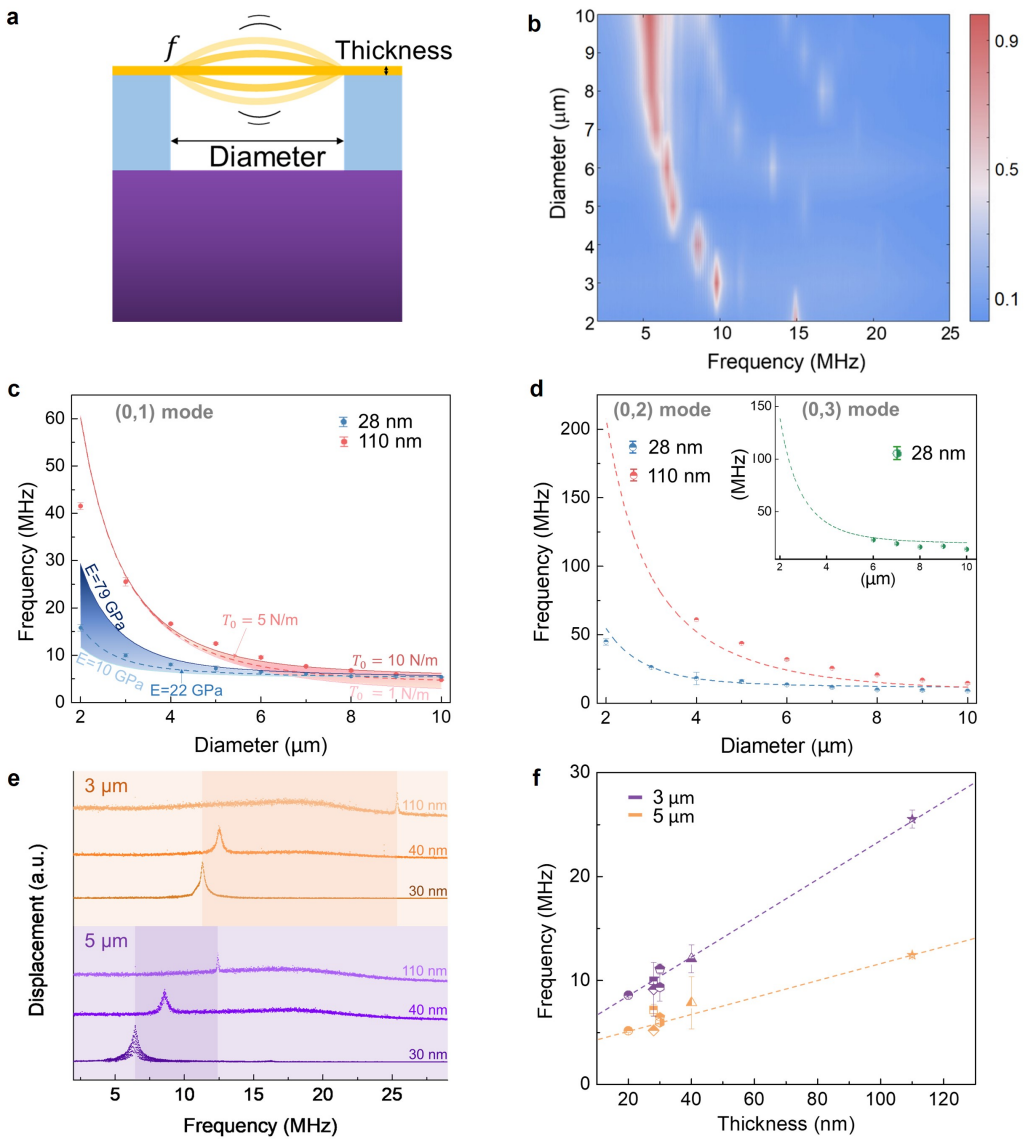

Figure 3: Thickness and radius dependence of the resonance frequencies of circular drums.(a) Sideview of the drum resonator and the key parameters studied. (b) Spectra taken in the centres of gold nanodrums of diameters ranging from 2 μm to 10 μm. Drumhead thickness is 28 nm. From 0-25 MHz, three modes can be identified. The dependence of the frequencies on the diameter is fitted using the stretched plate model of the (c) (0,1) modes and (d) (0,2) and (0,3) modes. Two thickness of the gold films used are 28 nm and 110 nm. (e) The vibration spectra of the (0,1) mode taken in the centres of the drums with different thicknesses (30 nm, 40 nm and 110 nm). Two diameters are chosen: 3 μm (bisque) and 5 μm (purple). The darker shadows show the shift in peak frequencies. (f) Thickness dependence of the (0,1) modes of drums with diameters 3 μm and 5 μm. The dashed lines show the trends in the shift, rather than a linear relationship. Error bars are standard deviations of frequencies measured from 5 samples with the same diameter and thickness. All the spectra shown in this figure were taken at zero gate voltage. A periodic chirp signal of amplitude 5 V and offset 5 V was applied to the surfaces to amplify the signals.

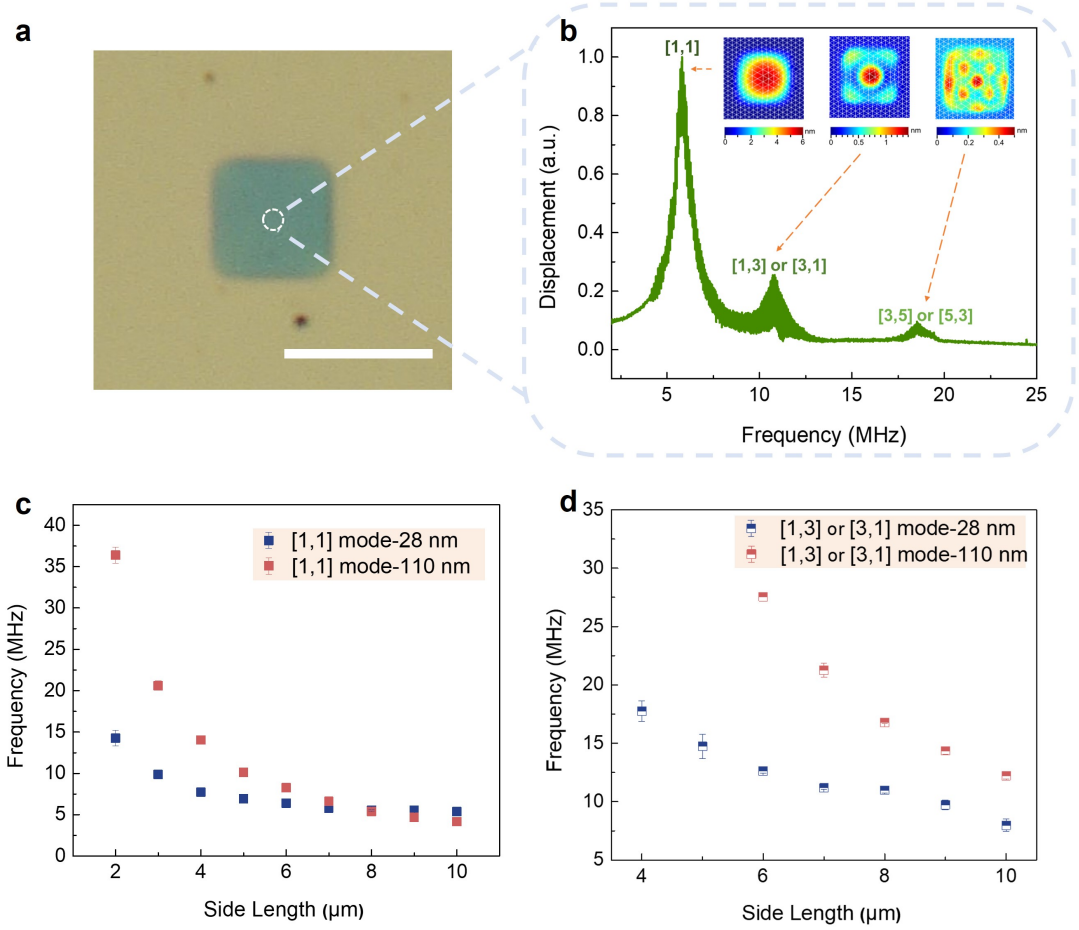

Figure 4: Vibration spectra of square drums. (a) The optical image of a square drum resonator. Scalebar: 10 μm. (b) The resonance spectrum taken at the centre of the square drum shown in (a). The side length of the square is 7 μm and the thickness of the gold film is 28 nm. Three modes can be seen in the frequency range from 0 - 25 MHz. The mode orders were determined from the resonance profile reconstructed from the scanning process. Inset: mode shapes at different resonance frequencies. (c) The frequencies of the [1,1] mode of different side lengths. (d) The frequencies of the [1,3] or [3,1] mode of different side lengths. Error bars are standard deviations of frequencies measured from 5 samples with the same side length and thickness. All the spectra shown in this figure were taken at zero gate voltage. A periodic chirp signal of amplitude 5 V and offset 5 V was applied to the surfaces to enhance the eigenfrequencies.

to a Q factor > 230. The highest Q factor we measured from the fundamental mode was from a circular drum with a thickness of 110 nm and diameter of 4 microns ($Q \sim 293$). The Q factors of our resonators are shown in Table S2 and it is evident that they are similar in magnitude to those reported using both resonance frequency methods and nanomechanical methods. It is well known that lowering the temperature[32]and the surrounding pressure[33] can significantly improve the Q factor. The fact that we carry out the measurement in ambient and room temperature shows that the quality of our drum is quite high. One possible reason for the Q factors of our drums being lower than some room temperature TMDC resonators may be due to the fact that the Young's modulus of gold is lower than graphene and TMDCs.[34]

Figure 5 (b) and (c) show the size dependence of the Q factors of drums in both square and circular shapes with thicknesses of 28 nm and 110 nm. Though some fluctuations exist, it is evident that the Q factor increases as the size decreases, which is consistent with the trend in the vibration frequencies. For similar sizes of the drum, the shape of the drumhead is not a critical factor. Figure 5 (d) shows the Q-factors of 100 circular drums of different diameters (0-9 µm) and thicknesses (20 nm, 28 nm, 38 nm, 40 nm, 110 nm). We can see that the Q-factor consistently increases with increasing thickness and decreases with increasing diameter. This is probably due to the fact that the films become more plate like and gas damping is decreased as a loss mechanism. The trends we observe are similar to those seen with micron-scale resonators based on 2D films of WSe_2 as well,[28] although the authors in those manuscripts did not comment much on that dependence. We believe such contradictory conclusions indicate that the dissipation mechanisms in micron-scale resonators still require comprehensive study.

In principle, the drum resonators may function as mass detectors. Assuming that the spring constant of the drum head is the same with and without a small load, the sensitivity of the resonator can be estimated as[35]

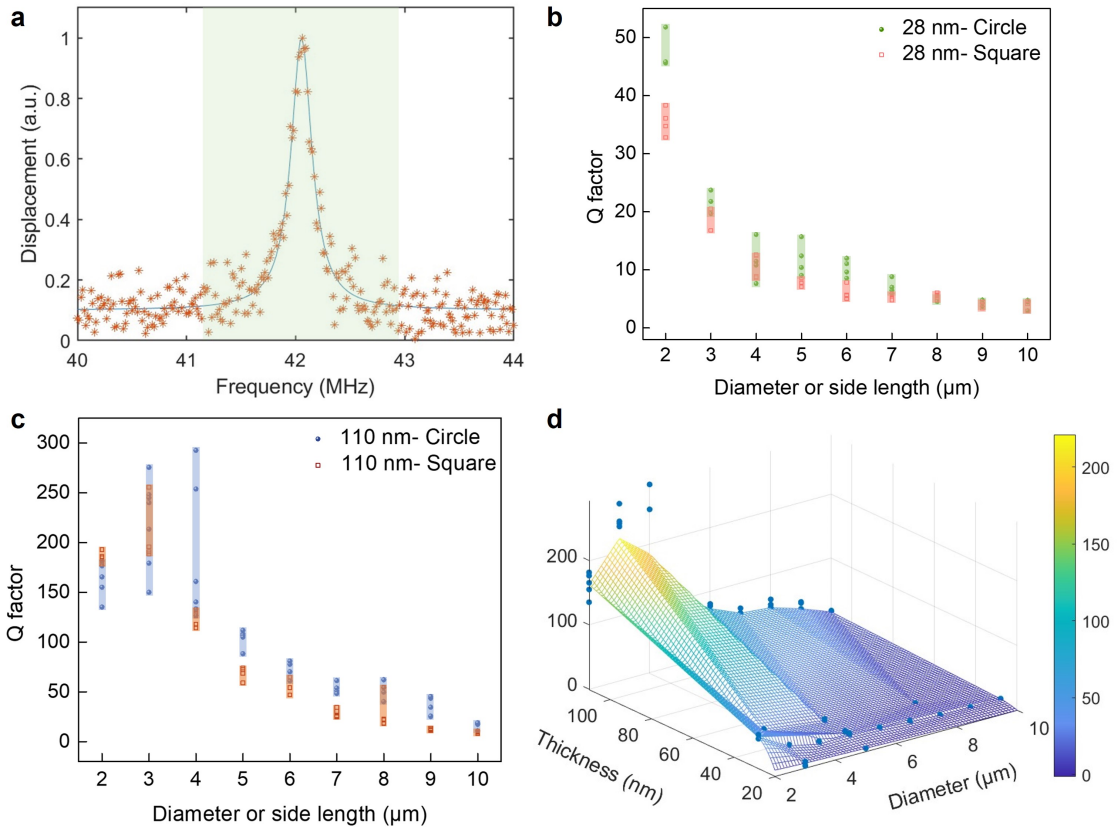

Figure 5: Quality factors and size and shape dependence. (a) The (0,1) mode resonance peak of a gold drum resonator and the corresponding Q factors. The diameter of the drum is 2 microns and the thickness of the drumhead is 110 nm. The solid line is the Lorentzian fit. (b) The Q factors of drums in the shape of circles and squares with a thickness of 28 nm as a fuction of size. (c) The Q factors of circular and square drums with a drumhead thickness of 28 nm as a function of size. (d) The Q factors of 100 drums of various size and film thickness. The meshed surface is constructed by interpolation using Matlab. All of the measurements in this figure were taken at zero back voltage. The driving signal was a periodic chirp signal of amplitude 5 V and offset 5 V.

$$\frac{\delta m}{\delta f} = \frac{2m_{\text{eff}}}{f_0}, \tag{5}$$

where m_{eff} is the effective mass, f_0 is the resonant frequency of the resonator.

For the fundamental mode of a drum resonator with the edges clamped, the effective mass can be written as[36]

$$m_{\text{eff}} = \frac{14}{27}\rho h \pi R^2, \tag{6}$$

where R is the radius of the drum. For our 28 nm resonators with a diameter of 10 µm, whose average resonance frequency is 5.42 MHz, the corresponding sensitivity should approach 8.12×10^{-21} gHz^{-1}. Since the vibration frequencies scale inversely with the radius, the sensitivity increases as the size decreases. The effective mass is proportional to the thickness. Since the vibration behaviour of the drums is dependent on the value of $\mathcal{A}$, the thickness dependence of the sensitivity is complicated and dependent on the individual drum. We have plotted the sensitivity of the 28 nm and 110 nm thick drums with diameters of 2-10 µm in Figure **S12**. It can be seen that the drum with a thickness of 28 nm and a diameter of 2 µm gives the highest sensitivity, i.e., 1.11×10^{-22} gHz^{-1}. This sensitivity is about 2 orders of magnitude higher than most silicon-based resonators[37] and is comparable to some graphene-based ones.[14]

While the drums exhibit vibrations whose natural resonance frequencies are determined by the tension and the flexural rigidity of the drumhead, they can be driven at any frequency by appplying suitable input electrical signals.

Figure **S13** shows the response of a 28 nm-thick drum with a diameter of 10 µm driven by a pure sine wave electronic signals with frequencies of 6 MHz, 12 MHz and 20 MHz. It can be seen that no distortion is detected between the input and output signals. The output peak is identical to the input one. Hence, the drum resonators may be very useful opto-mechanical converters. Due to the inert nature of gold, our device also shows excellent

robustness and stability. The drums were stored in ambient conditions. After 11 months of storage, no discernible shift of the first and second modes could be detected, as shown in Figure **S14**.

Conclusions

We have developed a nanodrum resonator system operating in the MHz frequency range using nanometre-thick gold films as the drumhead. The drum can be fabricated into different sizes, thicknesses and shapes, and compositions, enabling us to perform a systematic study of the mechanical response of the drum in both the plate and membrane regimes. The drums exhibit high quality factors at room temperature and standard atmospheric pressure. The drums can be driven by external sinusoidal electronic signals of arbitrary frequency as well. No distortion between the input and output signals is detected in the MHz regime. The stretched plate model is used to describe the natural vibrations of the gold drums. The Q-factor increases with increasing thickness of the drumheads and with decreasing drum diameter. The highest Q-factor measured is over 290 for the first mode. The drums can also be driven by an arbitrary external electronic signal. The output signal from the drum shows no distortion from the input signal in the MHz regime. The drum resonators also exhibit great stability and robustness, with no change in the resonance frequency over 11 months ($\pm$ 0.5 %). When acting as a mass sensor, the sensitivity is predicted to be as high as 10^{-1} zeptogram per Hertz. This nanodrum fabricated based on thin metal films is more robust than typical 2D based drum resonators. Experiments to confirm this are underway.

Methods

Sample Fabrication

The fabrication process of the gold nanodrum consisted of two major steps, i.e., substrate patterning and gold film transfer.

Substrate Patterning The substrates were fabricated by photolithography and reactive ion etching. We first grew a layer of SiO_2 (the thickness depends on the desired depth of the cavity) using PECVD (Plasma Enhanced Chemical Vapour Deposition, Oxford Instruments PLASMALAB 100 PECVD) on the polished side of a piece of silicon wafer (0.5µm uncoated, n-type, phosphorus doped, 1-10 Ohm SSP). Then we spin coated photoresist (AZ1512) on top of the SiO_2 at 3000 rpm for 30 s (Laurell Spinner), followed by a hotplate softbake of 2 minutes at 110 °C. We then exposed the photoresist to 75mj/cm^2 of 365nm UV light using a mask aligner (SUSS MA6) and appropriate Chrome/Glass photomask for pattern transfer. Next, the photoresist was developed using AZ736MIF until the UV exposed portion of the resist was fully removed to produce the pattern. Afterwards, the patterned photoresist acted as the protection layer for etching (Oxford Instruments PLASMALAB100 ICP380) the exposed SiO_2 layer. The remaining masking resist was removed using O_2 plasma to achieve a clean SiO_2 surface to accept the gold film which will ultimately form the drum.

Gold Film Transfer The flow chart for the gold film transfer is shown in Figure **S2**. First, a layer of gold film of the desired thickness was deposited on the SiO_2 side of a Si/SiO_2 substrate using sputter coating (Quorum Q150T S). Then we spin coated (Laurel, WS-650SZ-6NPP/LITE) a layer of PMMA (4 wt % in ethyl acetate; PMMA: Aldrich, 182265-25G; Ethyl acetate: EMSURE, 1.09623.2511) on top as supporting layer. After the PMMA had cured, we stuck a piece of polydimethylsiloxane (PDMS, Dowsil SYLGARD Industrial 184 Silicone Elastomer KIT 0.5KG) onto the frame as a handle. Then we dissolved the SiO_2 with strong base (10 wt% NaOH water solution). When the gold/PMMA/PDMS film had totally detached from the substrate, we used the handle to transfer it to deionised water and rinsed the film for more than 2 hours to remove the base residue. Then we transferred it onto the patterned substrate and let it dry overnight, followed by a baking session at 100 °C to render a better adhesion. Finally we transferred the sample to acetone (AA008-

2.5L-J, Chem Supply) and the PMMA was dissolved and the PDMS detached simultaneously.

Characterisation

Optical Microscopy Optical Microscopic images were taken using a Hirox HRX-01 3D digital microscope.

Atomic Force Microscopy AFM measurements were carried out on an Asylum Research MFP-3D Atomic Force Microscope. All measurements were performed in the standard tapping mode with AC160TS-R3 tips from Oxford Instruments.

Vibration Spectra Vibration spectra were collected with two vibrometers according to the frequency range needed. For measurements in the range of 0-25 MHz, we used a Polytech MSA-400 and all the signals applied to the drumheads were from the Vibrometers built in signal generator. For measurements above 25 MHz and no higher than 120 MHz, we used Polytech UHF-120, and the driving signals were generated by SMBV100A vector signal generator from Rohde & Schwarz.

Micropositioner and Probe The micropositioner used to apply the signal to the gold film was a FormFactor DPP 210, coaxial cable. The probe tip was a PTC-12-25 Specialty probe tip, composed of tungsten carbide.

Scanning Electron Microscopy SEM imaging was carried out using a Hitachi FlexSEM.

Modelling

Resonance mode shape modelling Resonance mode shape modelling was performed using COMSOL Multiphysics. For the resonance modes shown in Figure **S7**, the parameters used were: Young's modulus E = 79 GPa, Poisson Ratio $\nu = 0.425$, gold density = 19.25 g/cm^3, diameter $d = 10$ µm, thickness $h = 30$ nm and the inbuilt tension $T = 3$ N/m.

Acknowledgement

This work was supported by grants from the ARC (CE170100026, DP160102754) and the Department of Industry (ACSRIII00001).This work was performed in part at the Melbourne Centre for Nanofabrication (MCN) in the Victorian Node of the Australian National Fabrication Facility (ANFF). We appreciate the assistance and suggestions from J. Hutchison and Y. Ji from the University of Melbourne, and the discussion with C. Nie from Chongqing Institute of Green and Intelligent Technology.

Author Contributions

Jialu Li: Concept, Data Collection, Data Interpretation and Analysis, Modelling, Figure Preparation, Drafting and Review of Manuscript.
Ash Dyer and Dan Smith: Data Collection, Instrument Development, Data Analysis, and Review of Manuscript.
Paul Mulvaney: Concept, Funding and Resourcing, Supervision, Data Analysis, Drafting and Review of Manuscript.

Supporting Information Available

Supporting Figures, details on the stretched plate model, eigenfrequencies of square drum vibrations and the Supporting Tables.

References

(1) Lassagne, B.; Garcia-Sanchez, D.; Aguasca, A.; Bachtold, A. Ultrasensitive mass sensing with a nanotube electromechanical resonator. *Nano Letters* **2008**, *8*, 3735–3738.

(2) Erdogan, R. T.; Alkhaled, M.; Kaynak, B. E.; Alhmoud, H.; Pisheh, H. S.; Kelleci, M.;

Karakurt, I.; Yanik, C.; Sen, Z. B.; Sari, B., et al. Atmospheric pressure mass spectrometry of single viruses and nanoparticles by nanoelectromechanical systems. *ACS Nano* **2022**, *16*, 3821–3833.

(3) Fan, X.; Forsberg, F.; Smith, A. D.; Schroder, S.; Wagner, S.; Ostling, M.; Lemme, M. C.; Niklaus, F. Suspended graphene membranes with attached silicon proof masses as piezoresistive nanoelectromechanical systems accelerometers. *Nano Letters* **2019**, *19*, 6788–6799.

(4) Nazir, S.; Kwon, O. S., et al. Micro-electromechanical systems-based sensors and their applications. *Appl. Sci. Converg. Technol* **2022**, *31*, 40–45.

(5) Schlicke, H.; Battista, D.; Kunze, S.; Schroter, C. J.; Eich, M.; Vossmeyer, T. Free-standing membranes of cross-linked gold nanoparticles: novel functional materials for electrostatic actuators. *ACS Applied Materials & Interfaces* **2015**, *7*, 15123–15128.

(6) Erbil, S. O.; Hatipoglu, U.; Yanik, C.; Ghavami, M.; Ari, A. B.; Yuksel, M.; Hanay, M. S. Full electrostatic control of nanomechanical buckling. *Physical Review Letters* **2020**, *124*, 046101.

(7) Middlemiss, R.; Samarelli, A.; Paul, D.; Hough, J.; Rowan, S.; Hammond, G. Measurement of the Earth tides with a MEMS gravimeter. *Nature* **2016**, *531*, 614–617.

(8) Sazonova, V.; Yaish, Y.; Üstünel, H.; Roundy, D.; Arias, T. A.; McEuen, P. L. A tunable carbon nanotube electromechanical oscillator. *Nature* **2004**, *431*, 284–287.

(9) Deng, G.-W.; Zhu, D.; Wang, X.-H.; Zou, C.-L.; Wang, J.-T.; Li, H.-O.; Cao, G.; Liu, D.; Li, Y.; Xiao, M., et al. Strongly coupled nanotube electromechanical resonators. *Nano Letters* **2016**, *16*, 5456–5462.

(10) Husain, A.; Hone, J.; Postma, H. W. C.; Huang, X.; Drake, T.; Barbic, M.; Scherer, A.;

Roukes, M. Nanowire-based very-high-frequency electromechanical resonator. *Applied Physics Letters* **2003**, *83*, 1240–1242.

(11) Feng, X.; He, R.; Yang, P.; Roukes, M. Very high frequency silicon nanowire electromechanical resonators. *Nano Letters* **2007**, *7*, 1953–1959.

(12) He, R.; Feng, X.; Roukes, M.; Yang, P. Self-transducing silicon nanowire electromechanical systems at room temperature. *Nano Letters* **2008**, *8*, 1756–1761.

(13) Bunch, J. S.; Van Der Zande, A. M.; Verbridge, S. S.; Frank, I. W.; Tanenbaum, D. M.; Parpia, J. M.; Craighead, H. G.; McEuen, P. L. Electromechanical resonators from graphene sheets. *Science* **2007**, *315*, 490–493.

(14) Zang, X.; Zhou, Q.; Chang, J.; Liu, Y.; Lin, L. Graphene and carbon nanotube (CNT) in MEMS/NEMS applications. *Microelectronic Engineering* **2015**, *132*, 192–206.

(15) Fan, X.; Forsberg, F.; Smith, A. D.; Schröder, S.; Wagner, S.; Rödjegård, H.; Fischer, A. C.; Östling, M.; Lemme, M. C.; Niklaus, F. Graphene ribbons with suspended masses as transducers in ultra-small nanoelectromechanical accelerometers. *Nature Electronics* **2019**, *2*, 394–404.

(16) Chen, C.; Hone, J. Graphene nanoelectromechanical systems. *Proceedings of the IEEE* **2013**, *101*, 1766–1779.

(17) Klimov, N. N.; Jung, S.; Zhu, S.; Li, T.; Wright, C. A.; Solares, S. D.; Newell, D. B.; Zhitenev, N. B.; Stroscio, J. A. Electromechanical properties of graphene drumheads. *Science* **2012**, *336*, 1557–1561.

(18) Lee, J.; Wang, Z.; He, K.; Shan, J.; Feng, P. X.-L. High frequency MoS_2 nanomechanical resonators. *ACS Nano* **2013**, *7*, 6086–6091.

(19) Lee, J.; Wang, Z.; He, K.; Yang, R.; Shan, J.; Feng, P. X.-L. Electrically tunable single- and few-layer MoS_2 nanoelectromechanical systems with broad dynamic range. *Science Advances* **2018**, *4*, eaao6653.

(20) Ye, F.; Lee, J.; Feng, P. X.-L. Atomic layer MoS_2-graphene van der Waals heterostructure nanomechanical resonators. *Nanoscale* **2017**, *9*, 18208–18215.

(21) Smith, A. D.; Niklaus, F.; Paussa, A.; Schroder, S.; Fischer, A. C.; Sterner, M.; Wagner, S.; Vaziri, S.; Forsberg, F.; Esseni, D., et al. Piezoresistive properties of suspended graphene membranes under uniaxial and biaxial strain in nanoelectromechanical pressure sensors. *ACS Nano* **2016**, *10*, 9879–9886.

(22) Huang, S.; Dakhchoune, M.; Luo, W.; Oveisi, E.; He, G.; Rezaei, M.; Zhao, J.; Alexander, D. T.; Züttel, A.; Strano, M. S., et al. Single-layer graphene membranes by crack-free transfer for gas mixture separation. *Nature Communications* **2018**, *9*, 1–11.

(23) Mueggenburg, K. E.; Lin, X.-M.; Goldsmith, R. H.; Jaeger, H. M. Elastic membranes of close-packed nanoparticle arrays. *Nature Materials* **2007**, *6*, 656–660.

(24) Kanjanaboos, P.; Lin, X.-M.; Sader, J. E.; Rupich, S. M.; Jaeger, H. M.; Guest, J. R. Self-assembled nanoparticle drumhead resonators. *Nano Letters* **2013**, *13*, 2158–2162.

(25) Suzuki, H.; Yamaguchi, N.; Izumi, H. Theoretical and experimental studies on the resonance frequencies of a stretched circular plate: Application to Japanese drum diaphragms. *Acoustical Science and Technology* **2009**, *30*, 348–354.

(26) Neugebauer, C. Tensile properties of thin, evaporated gold films. *Journal of Applied Physics* **1960**, *31*, 1096–1101.

(27) Weihs, T.; Hong, S.; Bravman, J.; Nix, W. Mechanical deflection of cantilever microbeams: A new technique for testing the mechanical properties of thin films. *Journal of Materials Research* **1988**, *3*, 931–942.

(28) Zhu, J.; Xu, B.; Xiao, F.; Liang, Y.; Jiao, C.; Li, J.; Deng, Q.; Wu, S.; Wen, T.; Pei, S., et al. Frequency Scaling, Elastic Transition, and Broad-Range Frequency Tuning in WSe_2 Nanomechanical Resonators. *Nano Letters* **2022**, *22*, 5107–5113.

(29) Falin, A.; Holwill, M.; Lv, H.; Gan, W.; Cheng, J.; Zhang, R.; Qian, D.; Barnett, M. R.; Santos, E. J.; Novoselov, K. S., et al. Mechanical properties of atomically thin tungsten dichalcogenides: WS_2, WSe_2, and WTe_2. *ACS Nano* **2021**, *15*, 2600–2610.

(30) Lee, M.; Davidovikj, D.; Sajadi, B.; Siskins, M.; Alijani, F.; Van Der Zant, H. S.; Steeneken, P. G. Sealing graphene nanodrums. *Nano Letters* **2019**, *19*, 5313–5318.

(31) Lee, C.; Wei, X.; Kysar, J. W.; Hone, J. Measurement of the elastic properties and intrinsic strength of monolayer graphene. *Science* **2008**, *321*, 385–388.

(32) Morell, N.; Reserbat-Plantey, A.; Tsioutsios, I.; Schadler, K. G.; Dubin, F.; Koppens, F. H.; Bachtold, A. High quality factor mechanical resonators based on WSe_2 monolayers. *Nano Letters* **2016**, *16*, 5102–5108.

(33) Lee, J.; Wang, Z.; He, K.; Shan, J.; Feng, P. X.-L. Air damping of atomically thin MoS_2 nanomechanical resonators. *Applied Physics Letters* **2014**, *105*, 023104.

(34) Zalalutdinov, M. K.; Robinson, J. T.; Junkermeier, C. E.; Culbertson, J. C.; Reinecke, T. L.; Stine, R.; Sheehan, P. E.; Houston, B. H.; Snow, E. S. Engineering graphene mechanical systems. *Nano Letters* **2012**, *12*, 4212–4218.

(35) Wong, C.; Annamalai, M.; Wang, Z.; Palaniapan, M. Characterization of nanomechanical graphene drum structures. *Journal of Micromechanics and Microengineering* **2010**, *20*, 115029.

(36) Lei, X.-W.; Natsuki, T.; Shi, J.-X.; Ni, Q.-Q. An atomic-resolution nanomechanical mass sensor based on circular monolayer graphene sheet: theoretical analysis of vibrational properties. *Journal of Applied Physics* **2013**, *113*, 154313.

(37) Stassi, S.; Cooperstein, I.; Tortello, M.; Pirri, C. F.; Magdassi, S.; Ricciardi, C. Reaching silicon-based NEMS performances with 3D printed nanomechanical resonators. *Nature Communications* **2021**, *12*, 1–9.